Ciliary neurotrophic factor (CNTF) protects retinal cone and rod photoreceptors by suppressing excessive formation of the visual pigments

Received for publication, May 17, 2018, and in revised form, August 15, 2018 Published, Papers in Press, August 16, 2018, DOI 10.1074/jbc.RA118.004008

Songhua Li[‡], **Kota Sato**[‡], **William C. Gordon**[‡§], **Michael Sendtner**[¶], **Nicolas G. Bazan**[‡§], **and Minghao Jin**[‡§1]

From the [‡]*Neuroscience Center of Excellence and* [§]*Department of Ophthalmology, Louisiana State University School of Medicine, New Orleans, Louisiana 70112 and the* [¶]*Institute of Clinical Neurobiology, University Hospital Würzburg, D-97078 Würzburg, Germany*

Edited by George M. Carman

The retinal pigment epithelium (RPE)-dependent visual cycle provides 11-*cis*-retinal to opsins in the photoreceptor outer segments to generate functional visual pigments that initiate phototransduction in response to light stimuli. Both RPE65 isomerase of the visual cycle and the rhodopsin visual pigment have recently been identified as critical players in mediating light-induced retinal degeneration. These findings suggest that the expression and function of RPE65 and rhodopsin need to be coordinately controlled to sustain normal vision and to protect the retina from photodamage. However, the mechanism controlling the development of the retinal visual system remains poorly understood. Here, we show that deficiency in ciliary neurotrophic factor (CNTF) up-regulates the levels of rod and cone opsins accompanied by an increase in the thickness of the outer nuclear layers and the lengths of cone and rod outer segments in the mouse retina. Moreover, retinoid isomerase activity, expression levels of RPE65 and lecithin:retinol acyltransferase (LRAT), which synthesizes the RPE65 substrate, were also significantly increased in the *Cntf*$^{-/-}$ RPE. Rod *a*-wave and cone *b*-wave amplitudes of electroretinograms were increased in *Cntf*$^{-/-}$ mice, but rod *b*-wave amplitudes were unchanged compared with those in WT mice. Up-regulated RPE65 and LRAT levels accelerated both the visual cycle rate and recovery rate of rod light sensitivity in *Cntf*$^{-/-}$ mice. Of note, rods and cones in *Cntf*$^{-/-}$ mice exhibited hypersusceptibility to light-induced degeneration. These results indicate that CNTF is a common extracellular factor that prevents excessive production of opsins, the photoreceptor outer segments, and 11-*cis*-retinal to protect rods and cones from photodamage.

Phototransduction that converts light energy into electrical impulse in the retina begins with photoisomerization of 11-*cis*-retinal (11*c*RAL)[2] to all-*trans*-retinal in the opsin visual pigments localized to the outer segments (OS), the light-sensing organelles, of rod and cone photoreceptors (1, 2). Because apoopsins without the 11*c*RAL chromophore are not responsive to light, 11*c*RAL must be regenerated and recombined with apoopsins to form light-sensitive visual pigments in the photoreceptor OS. RPE65 is a key retinoid isomerase in the RPE-dependent visual cycle responsible regenerating 11*c*RAL (3–5). It catalyzes synthesis of 11-*cis*-retinol, the reduced form of 11*c*RAL, from all-*trans*-retinyl esters synthesized by LRAT and other enzymes in the RPE (6–8).

Although rhodopsin is essential for initiating rod phototransduction it is also the mediator of rod degeneration induced by intense light (9). In addition, higher expression level and activity of RPE65 are associated with an increase in susceptibility of the photoreceptors to light-induced degeneration (10–12). These findings suggest that the expression levels and function of rhodopsin and RPE65 need to be controlled to maintain normal vision and to protect photoreceptors from light-induced degeneration. However, the molecular mechanisms that coordinately control expressions of both opsin and RPE65 during the development and maturation of the retinal light-sensing system remain largely unknown.

Expressed by Muller and RPE cells (13–15), CNTF is an extracellular signaling protein in the neuroretinal and the interphotoreceptor matrix, which is associated with the membranes of the RPE, Muller, and photoreceptor cells (16). CNTF initiates its signaling by interacting with its receptor-α, which then recruits the leukemia inhibitory factor (LIF) receptor-β and gp130 to form a functional receptor complex in the cell membrane (17). All of these receptor subunits are expressed in the RPE and photoreceptors (14, 18–20). Exogenous CNTF has

This work was supported by National Institutes of Health Grants EY021208 (to M. J.), GM103340 (to N. G. B.), and EY005121 (to N. G. B), Louisiana State University School of Medicine Research Enhancement Fund (to M. J.), and Interdisziplinäres Zentrum für Klinische Forschung Grant N-304 (to M. S.). The authors declare that they have no conflicts of interest with the contents of this article. The content is solely the responsibility of the authors and does not necessarily represent the official views of the National Institutes of Health.

[1] To whom correspondence should be addressed: Neuroscience Center, LSU School of Medicine, 2020 Gravier St., New Orleans, LA 70112. Tel.: 504-568-2141; Fax: 504-599-0891; E-mail: mjin@lsuhsc.edu.

[2] The abbreviations used are: 11*c*RAL, 11-*cis*-retinal; BC, bipolar cell; CAR, cone arrestin; CNTF, ciliary neurotrophic factor; DAPI, 4′,6′-diamidino-2-phenylindole; ERG, electroretinography; INL, inner nuclear layer; IRBP, interphotoreceptor retinoid-binding protein; LIF, leukemia inhibitory factor; LRAT, lecithin:retinol acyltransferase; mGluR6, metabotropic glutamate receptor 6; ONL, outer nuclear layer; OS, outer segments; PKCα, protein kinase Cα; RPE, retinal pigment epithelium; TUNEL, terminal deoxynucleotidyl transferase dUTP nick end labeling; STAT, signal transducers and activators of transcription; PI3K, phosphatidylinositol 3-kinase; FBS, fetal bovine serum; PB, phosphate buffer; DMEM, Dulbecco's modified Eagle's medium; cd $\times$ s/m^2, candelas $\times$ s per m^2; Rho, rhodopsin; OPL, outer plexiform layer; ROS, rod outer segments; MAPK, mitogen-activated protein kinase.

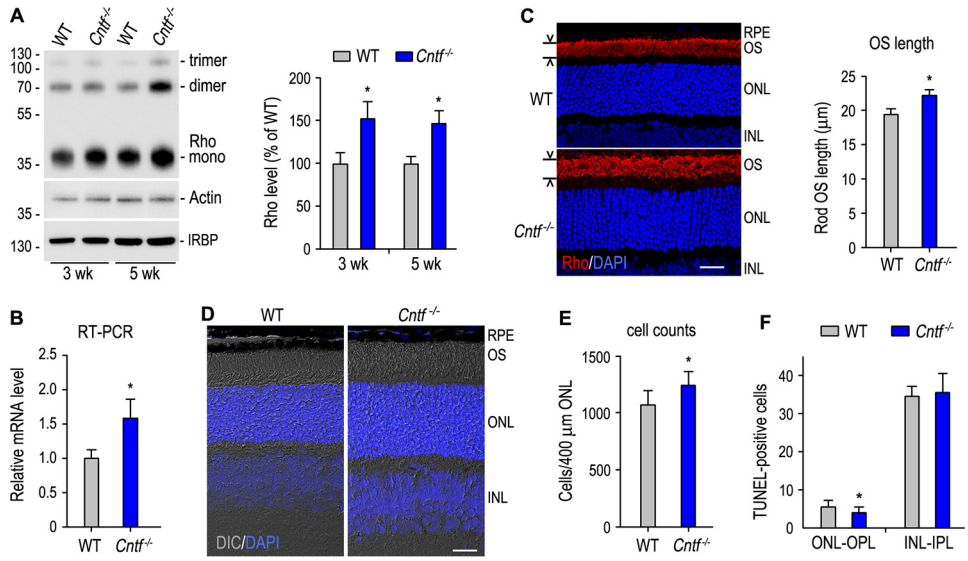

Figure 1. Increase in rhodopsin (*Rho*) expression, thickness of the ONL, and length of rod OS in *Cntf*$^{-/-}$ mouse. *A*, immunoblot analysis of Rho and IRBP in 3- and 5-week-old WT and *Cntf*$^{-/-}$ retinas. Actin was detected to normalize sample loading. The histogram shows percentages of the immunoblot intensities of Rho from *Cntf*$^{-/-}$ retinas relative to the Rho immunoblot intensities of WT retinas. *Asterisks* in this figure indicate significant differences between WT and *Cntf*$^{-/-}$ mice ($p \leq 0.05$); *error bars* indicate S.D. ($n \geq 3$). *B*, transcription level of Rho mRNA in 3-week-old *Cntf*$^{-/-}$ retina was determined by quantitative RT-PCR and expressed as fold of Rho mRNA in age-matched WT retina. *C*, immunohistochemistry showing localization of Rho (*red*) to the rod OS in the superior retinas of 3-week-old WT and *Cntf*$^{-/-}$ mice. Nuclei were stained with DAPI (*blue*). Histogram shows Rho-positive OS lengths in the sections. *D*, differential interference contrast (*DIC*) images of retinal sections from 3-week-old WT and *Cntf*$^{-/-}$ mice. All *scale bars* denote 20 μm. *E*, rod nuclear numbers counted in a 400-μm wide superior ONL area that is 600 μm away from the optic nerve head. *F*, TUNEL-positive cell numbers in the ONL-OPL and inner nuclear layer (*INL*)-inner plexiform layer (*IPL*) of retinal sections from WT and *Cntf*$^{-/-}$ mice at postnatal day 8.

been shown to inhibit rhodopsin expression in the rodent retina (21–23), but it induced expression of rod and cone opsins in the chick retina (24, 25). In addition, CNTF increased RPE cell survival and mitotic activity (26).

In animal models of retinal degeneration, CNTF treatment promoted photoreceptor survival (27–31) and regeneration of cone outer segments (32). Furthermore, recent clinical trials in patients with retinitis pigmentosa, Usher syndrome type 2, or geographic atrophy showed that CNTF treatment increased retinal thickness and slowed the progression of vision loss (33–35), although in some animal studies and human clinical trials CNTF treatment had no therapeutic benefit (36–38). Despite the neuroprotective effect in some clinical trials and animal studies, CNTF treatment significantly suppressed visual function, as determined by electroretinography (ERG) (29, 37, 39, 40). Intraocular CNTF administration also suppressed ERG responses in wildtype (WT) animals (23, 40–42).

A gene profiling study showed that intravitreal injection of CNTF induced numerous genes associated with inflammation and gliosis in the Muller cells (43). In addition, CNTF increased secretion of neurotrophin-3 and decreased secretion of vascular endothelial growth factor, interleukin-8, and transforming growth factor-β2 in the RPE cells (14). These altered gene expression and protein secretion might cause many secondary effects in the CNTF-treated patients and animals, and therefore, increased difficulty in defining the primary role and mechanism of CNTF function in regulating development, function, and protection of the retinal photoreceptors and RPE. In this study, we analyzed neuroretinal and RPE phenotypes in *Cntf*$^{-/-}$ mice, and identified CNTF as a common extracellular signal that down-regulates expression of opsins in rod and cone photoreceptors, as well as RPE65 and LRAT in the RPE, to avoid excessive formation of both light-sensing organelles and light-sensitive visual pigments, which mediate phototransduction or photoreceptor degeneration, depending on the light intensity they have captured.

Results

Rod excessive development is associated with up-regulation of rhodopsin in the Cntf$^{-/-}$ *retina*

CNTF added into retinal cultures displayed distinct effects on rod development depending on species: it promoted chick rod development and rod-opsin expression (24), but it inhibited rat rod differentiation and rod-opsin expression (21). To define the effect of CNTF deficiency on rod development and rod-opsin expression, we first compared expression levels of rhodopsin in WT and *Cntf*$^{-/-}$ mice. As shown in Fig. 1*A*, expression levels of rhodopsin (Rho) in 3- and 5-week-old *Cntf*$^{-/-}$ mice were 45–50% higher than those in age-matched WT mice. Rho mRNA expression levels in 3-week-old *Cntf*$^{-/-}$ retina were increased by ~53% as compared with those in the same age WT retina (Fig. 1*B*).

To confirm these results, we analyzed morphology of WT and *Cntf*$^{-/-}$ retinas. Immunohistochemistry showed that length of the rod outer segments (ROS) in a 3-week-old *Cntf*$^{-/-}$ mouse was 15% longer than that of WT mouse (Fig. 1*C*). Differential interference contrast microscopy of retinal sections confirmed that both ROS length and thickness of the outer nuclear layer (ONL) in 3-week-old *Cntf*$^{-/-}$ retina are clearly greater than those in age-matched WT retina (Fig. 1*D*). To know if numbers of rods are increased in the *Cntf*$^{-/-}$ mouse, we counted nuclear numbers in a 400-μm wide region of the superior ONL that is 600 μm away from the optic nerve head. As

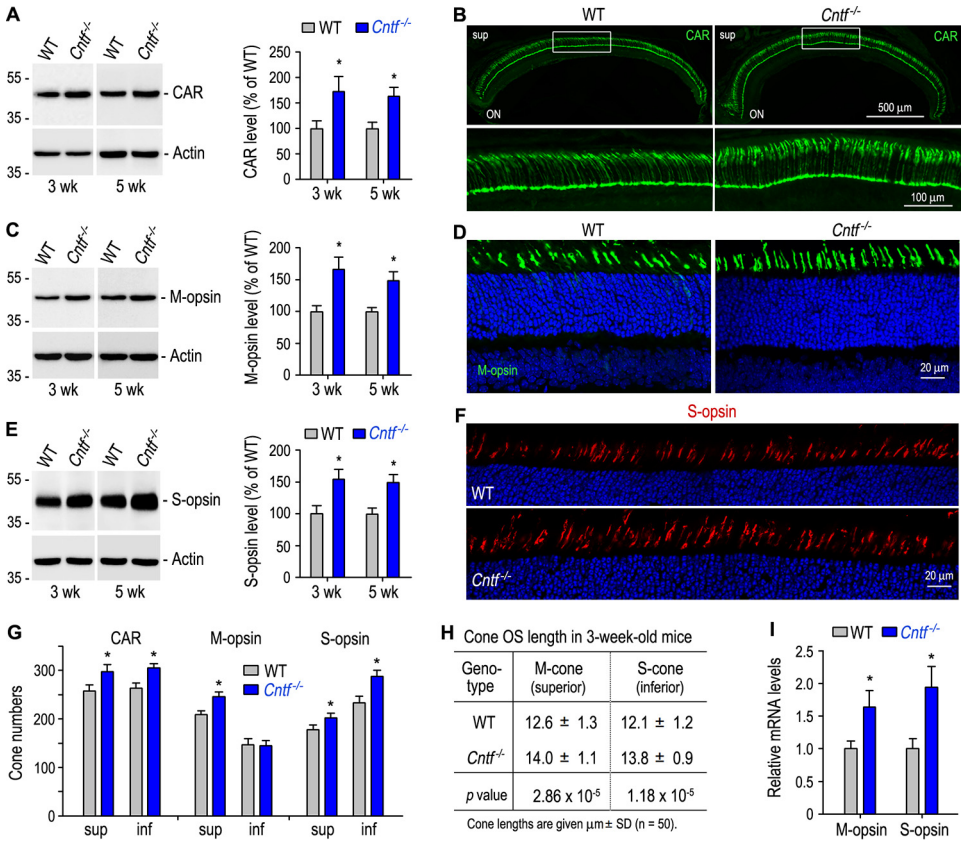

Figure 2. Increase in expression of cone-specific proteins and length of cone OS in *Cntf*$^{-/-}$ mouse. *A,* immunoblot analysis of CAR in the retinas of 3- or 5-week-old WT and *Cntf*$^{-/-}$ mice. The histogram shows percentages of immunoblot intensities of CAR from *Cntf*$^{-/-}$ retinas relative to the CAR immunoblot intensities of WT retinas. *B,* immunohistochemistry showing CAR immunoreactivity in the superior (*sup*) retinas of 3-week-old WT and *Cntf*$^{-/-}$ mice (*upper panels*). *ON*, optic nerve. The areas of the rectangles are shown in the higher magnification images (*bottom panels*). *C* and *E,* immunoblot analysis of M-opsin (*C*) and S-opsin (*E*) from 3- or 5-week-old WT and *Cntf*$^{-/-}$ retinas. Histograms show percentages of immunoblot intensities of M-opsin (*C*) or S-opsin (*E*) in the *Cntf*$^{-/-}$ retinas relative to M-opsin or S-opsin intensities in WT retinas. *D* and *F*, immunohistochemistry for M-opsin (*D*) and S-opsin (*F*) in the superior (*D*) or inferior (*F*) retinas of 3-week-old WT and *Cntf*$^{-/-}$ mice. *G*, numbers of CAR- or cone opsin-positive cells in the superior (*sup*) or inferior (*inf*) retinas of 3-week-old WT and *Cntf*$^{-/-}$ mouse retinal sections taken from the dorsal-ventral midline of the eye. *H*, lengths of M- and S-cone OS in 3-week-old WT and *Cntf*$^{-/-}$ mouse retinal sections. *I*, relative mRNA levels of cone opsins in 3-week-old WT and *Cntf*$^{-/-}$ retinas were determined by quantitative RT-PCR. All *asterisks* indicate significant differences between WT and *Cntf*$^{-/-}$ mice ($p < 0.05$); *error bars* denote S.D. ($n = 3$~4).

shown in Fig. 1*E*, numbers of rods in the region of the *Cntf*$^{-/-}$ retina were 11% greater than those in WT retina. Numbers of TUNEL-positive cells in the ONL and the outer plexiform layer (OPL) of the *Cntf*$^{-/-}$ retina at postnatal day 8 were significantly smaller than those in age-matched WT retinal ONL-OPL (Fig. 1*F*).

Increase of cone-specific proteins in over-elongated OS of Cntf$^{-/-}$ *cones*

Exogenous CNTF has been shown to promote cone differentiation in the developing chick retina (24, 25), suggesting that CNTF deficiency may reduce expression of cone-specific proteins. Unexpectedly, quantitative immunoblot analysis showed that cone arrestin (CAR), which expresses in both M- and S-cones (44), was increased ~50% in 3- and 5-week-old *Cntf*$^{-/-}$ mouse retinas, as compared with age-matched WT mouse retinas (Fig. 2*A*). In agreement with this result, immunohistochemistry showed that length and numbers of CAR-positive outer segments in 3-week-old *Cntf*$^{-/-}$ retina were clearly greater than those in WT retina (Fig. 2, *B* and *G*).

To know whether M- and S-opsins are also increased in the *Cntf*$^{-/-}$ retina, we performed quantitative immunoblot analysis for cone opsins. As shown in Fig. 2, *C* and *E*, expression levels of M- and S-opsins in 3- and 5-week-old *Cntf*$^{-/-}$ retinas are significantly higher than those in age-matched WT retinas. This increase in expression of cone opsins is associated with an increase in M- and S-cone numbers as well as length of cone outer segments in the *Cntf*$^{-/-}$ retina (Fig. 2, *D* and *F–H*). Quantitative RT-PCR revealed that transcripts for M- and S-opsins were increased by 60~70% in 3-week-old *Cntf*$^{-/-}$ retina, as compared with those in age-matched WT retina (Fig. 2*I*).

Up-regulation of visual cycle enzymes in Cntf$^{-/-}$ *RPE*

Increased rod and cone opsins may need an increase in 11*c*RAL synthesis to form functional visual pigments. We therefore tested whether the visual cycle enzymes are changed in the *Cntf*$^{-/-}$ RPE. Immunoblot analysis showed that protein levels of RPE65 in 3- and 5-week-old *Cntf*$^{-/-}$ RPE were 40–60% higher than those in age-matched WT RPE (Fig. 3*A*). Similarly, expression levels of LRAT are also significantly increased in the *Cntf*$^{-/-}$ RPE, as compared with WT RPE (Fig. 3*B*). In agreement with these results, activities of the retinoid isomerase in the 3- and 5-week-old *Cntf*$^{-/-}$ RPE were at least 45% higher than those in age-matched WT RPE (Fig. 3*C*).

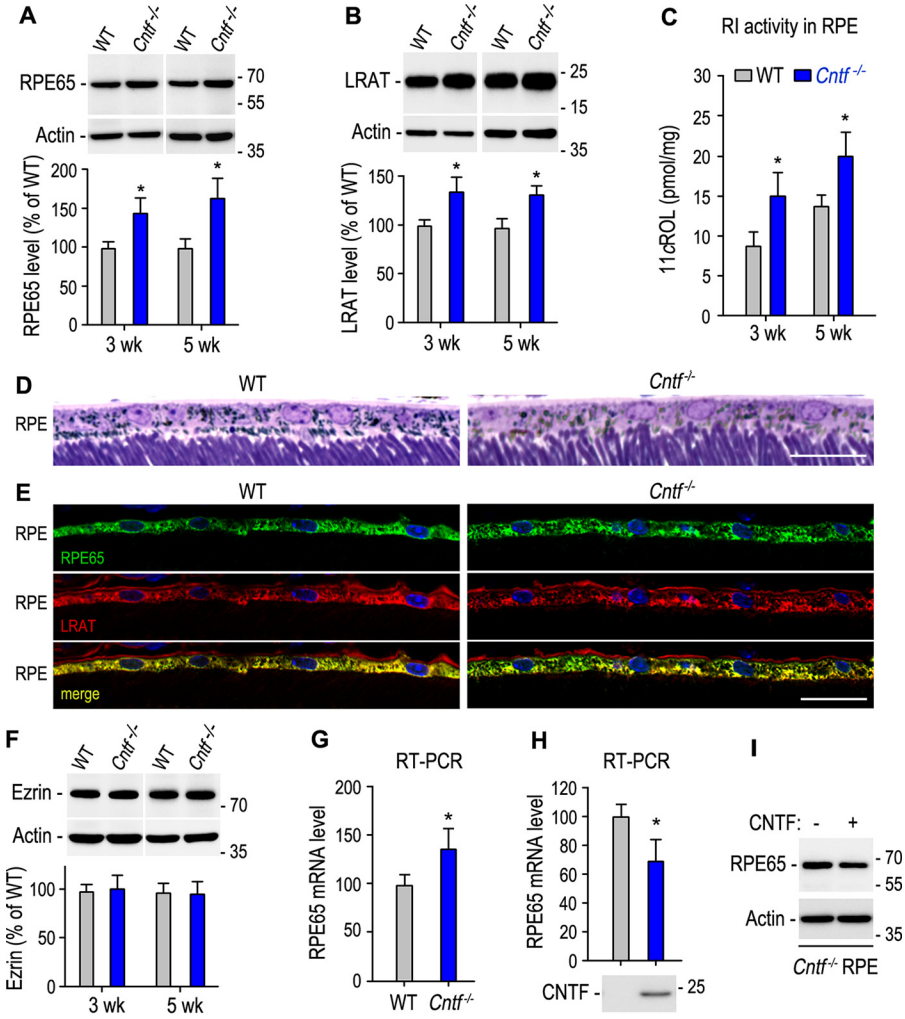

Figure 3. Up-regulation of the visual cycle enzymes in the *Cntf*$^{-/-}$ RPE. *A* and *B*, immunoblot analysis of RPE65 (*A*) and LRAT (*B*) in the RPE of 3- or 5-week-old WT and *Cntf*$^{-/-}$ mice. Histograms show immunoblot intensities of RPE65 or LRAT from the *Cntf*$^{-/-}$ RPE relative to RPE65 or LRAT intensities in WT mouse RPE. *C*, retinoid isomerase (*RI*) activities determined by measuring synthesis of 11*c*ROL from all-*trans*-retinol substrate incubated with RPE homogenates of 3- or 5-week-old WT and *Cntf*$^{-/-}$ mice. *D*, light microscopic images of RPE layers in the superior retinal sections of 5-week-old WT and *Cntf*$^{-/-}$ mice. *E*, immunohistochemistry showing distribution patterns of RPE65 and LRAT in the superior retinal sections from 3-week-old WT or *Cntf*$^{-/-}$ mice. *Scale bars* in *D* and *E* denote 20 μm. *F*, immunoblot analysis of Ezrin in the eyecups of 3- or 5-week-old WT and *Cntf*$^{-/-}$ mice. The histogram shows relative immunoblot intensities of Ezrin in WT and *Cntf*$^{-/-}$ eyecups. *G*, relative expression levels of RPE65 mRNA in WT and *Cntf*$^{-/-}$ RPE were determined by quantitative RT-PCR. *H*, quantitative RT-PCR showing relative expression levels of RPE65 mRNA in *Cntf*$^{-/-}$ mouse eyecup RPE incubated with media with or without CNTF. *I*, immunoblot analysis of RPE65 in *Cntf*$^{-/-}$ mouse eyecup RPE in *H*. All *asterisks* indicate significant differences between WT and *Cntf*$^{-/-}$ mice or between test and control groups ($p < 0.04$); *error bars* are S.D. ($n = 3$ or 4).

To know if the number of RPE cells is increased in *Cntf*$^{-/-}$ mouse, we counted DAPI-positive RPE nuclear numbers in sections taken from the dorsal-ventral midline of the eye. We then calculated RPE cell density by dividing RPE nuclear numbers with arc length of retina in the sections. RPE cell densities in *Cntf*$^{-/-}$ sections (28.6 ± 2.0 nuclei/mm, $n = 4$) were similar to those in WT sections (27.8 ± 1.8 nuclei/mm, $n = 4$). RPE morphology in the *Cntf*$^{-/-}$ retinal section was similar to that in WT retinal section (Fig. 3*D*). Distribution patterns of RPE65 and LRAT in the *Cntf*$^{-/-}$ RPE were also similar to those in WT RPE (Fig. 3*E*). Consistent with these results, expression levels of the RPE microvilli protein Ezrin in the *Cntf*$^{-/-}$ RPE were similar to those in WT RPE (Fig. 3*F*).

To determine whether CNTF up-regulates RPE65 expression at the transcription level we performed quantitative RT-PCR. As shown in Fig. 3*G*, mRNA expression levels of RPE65 were increased ~30% in the *Cntf*$^{-/-}$ mouse, as compared with WT mouse. To confirm this result, we incubated *Cntf*$^{-/-}$ eyecup RPE with media of 293T-LC cells transfected with pRK5 or pRK-CNTF. Quantitative RT-PCR and immunoblot analysis showed that both mRNA and protein levels of RPE65 were reduced in the eyecup RPE incubated with media containing CNTF (Fig. 3, *H* and *I*).

Rod hyperpolarization, but not rod ON bipolar depolarization, was increased in Cntf$^{-/-}$ *mouse*

Because rod-opsin is up-regulated in the *Cntf*$^{-/-}$ retina, we tested whether the *Cntf*$^{-/-}$ rods display an increased phototransduction. We recorded scotopic ERG responses of dark-adapted WT and *Cntf*$^{-/-}$ mice to a series of increasing light flashes. Representative ERG responses elicited with 0~2 log candelas × s/m^2 (cd × s/m^2) flashes are shown in Fig. 4*A*. Amplitudes of *a*-waves elicited with 1~2 log cd × s/m^2 flashes were significantly greater in *Cntf*$^{-/-}$ mice, as compared with

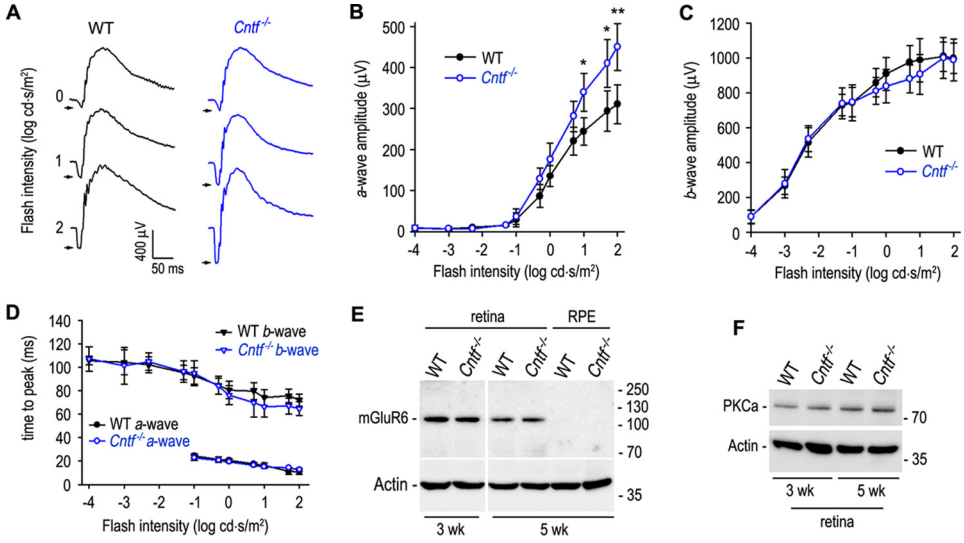

Figure 4. Enhanced rod phototransduction in *Cntf*$^{-/-}$ mice. *A*, representative raw scotopic ERG responses of dark-adapted WT and *Cntf*$^{-/-}$ mice to the indicated flashes. *B* and *C*, amplitudes of scotopic ERG *a*-wave (*B*) and *b*-wave (*C*) elicited with the indicated flashes in dark-adapted WT and *Cntf*$^{-/-}$ mice. *Asterisks* indicate significant differences between WT and *Cntf*$^{-/-}$ mice (*, $p < 0.04$; **, $p < 0.01$); *error bars* show S.D. ($n = 6$). *D*, times from stimulus onset to *a*- or *b*-wave peaks of WT and *Cntf*$^{-/-}$ mouse rods. *E*, immunoblot analysis of mGluR6 in 3- or 5-week-old WT and *Cntf*$^{-/-}$ mouse retinas or RPE. Actin was used as loading control. *F*, immunoblot analysis of PKCα in 3- or 5-week-old WT and *Cntf*$^{-/-}$ retinas.

those in WT mice (Fig. 4, *A* and *B*). Unexpectedly, *b*-wave amplitudes in *Cntf*$^{-/-}$ mice were similar to those of WT mice (Fig. 4, *A* and *C*).

To know if the synaptic function between rod and rod ON bipolar cell (ON-BC) was altered in the *Cntf*$^{-/-}$ mouse, we measured *a*- and *b*-wave implicit times (times from stimulus onset to *a*- or *b*-wave peak). As shown in Fig. 4*D*, *a*-wave implicit times of *Cntf*$^{-/-}$ rod ERG were similar to those of WT rod ERG. The *b*-wave implicit times of *Cntf*$^{-/-}$ rod ERG were also similar to those of WT rod ERG elicited with −4∼0 log cd × s/m^2 flashes. When 0.7∼1.7 log cd × s/m^2 flashes applied, the *b*-wave implicit times of *Cntf*$^{-/-}$ rod ERG were 10.5∼12.2% shorter than those of WT rods ($p = 0.056$, $n = 6$; Fig. 4*D*). Immunoblot analyses showed that expression levels of the ON-BC markers (mGluR6 and PKCα) in the *Cntf*$^{-/-}$ retina were similar to those in WT retina (Fig. 4, *E* and *F*).

Faster recovery rate of rod light sensitivity is underpinned by accelerated visual cycle in Cntf$^{-/-}$ *mouse*

Because rod opsin and the visual cycle enzymes are increased in the *Cntf*$^{-/-}$ mouse, we tested whether the recovery rate of rod light sensitivity is accelerated in *Cntf*$^{-/-}$ mouse. We exposed dark-adapted WT and *Cntf*$^{-/-}$ mice to 800 lux light for 5 min, and then returned the mice to darkness. At different times, we recorded scotopic ERG responses to three different flash stimuli (10, 25, and 50 cd × s/m^2). WT and *Cntf*$^{-/-}$ mice kept in darkness for 5 min displayed similar *a*-wave amplitudes (Fig. 5*A*). However, *a*-wave amplitudes of *Cntf*$^{-/-}$ mice kept in darkness for 10–30 min were higher than those in WT mice under the same light conditions (Fig. 5*A*).

To know if this faster recovery of rod light sensitivity is supported by an accelerated visual cycle, we measured the regeneration rates of 11*c*RAL in WT and *Cntf*$^{-/-}$ mice kept in darkness for different times after photobleaching the visual pigments. Because both the ONL thickness and the OS length are greater in *Cntf*$^{-/-}$ retina than those of WT retina, we expressed the levels of 11*c*RAL in photobleached WT and *Cntf*$^{-/-}$ eyes as 100%. After keeping the mice in darkness for 15 or 30 min, the amounts of 11*c*RAL were increased 55 or 83%, respectively, in *Cntf*$^{-/-}$ mice, but only 15 or 30% in WT mice (Fig. 5*B*). These data indicate that the regeneration rates of the 11*c*RAL in the *Cntf*$^{-/-}$ eyes are faster than those in the WT eyes.

Hyper visual function of cones in Cntf$^{-/-}$ *mouse*

The up-regulation of cone opsins in the *Cntf*$^{-/-}$ retina (Fig. 2) prompted us to test if cone visual function was enhanced in the *Cntf*$^{-/-}$ mouse. Under a rod-saturating background light, we recorded photopic ERG responses of WT and *Cntf*$^{-/-}$ mice to a series of increasing achromatic flashes. As shown in Fig. 6, *A–C*, amplitudes of *a*- and *b*-waves elicited with a given intensity of flash were significantly higher in *Cntf*$^{-/-}$ mice than WT mice. Implicit times to photopic *b*-wave peaks elicited with 0.5∼2 log cd × s/m^2 flashes were markedly shorter in *Cntf*$^{-/-}$ mice *versus* WT mice (Fig. 6*D*), suggesting that synaptic function between cone and cone ON-BC is normal or enhanced in *Cntf*$^{-/-}$ mice. To confirm these results, we recorded photopic flicker ERG. Consistent with the above results, amplitudes of *b*-waves elicited with 10- and 20-Hz flashes at 10 cd × s/m^2 intensity were significantly increased in *Cntf*$^{-/-}$ mice, as compared with those in WT mice (Fig. 6, *E* and *F*). These results indicate that CNTF deficiency causes a "super vision" mediated by cones. These results also suggest that CNTF may have different roles in the development and/or function of cone ON-BC *versus* rod ON-BC systems.

Rods and cones in Cntf$^{-/-}$ *mouse exhibited hyper susceptibility to photodamage*

Because the photoresponsiveness of rods and cones is increased in *Cntf*$^{-/-}$ mice, we investigated the effects of intense light on the retinal function and structure of *Cntf*$^{-/-}$ mice. We exposed mice to 12,000 lux light for different times (30∼75

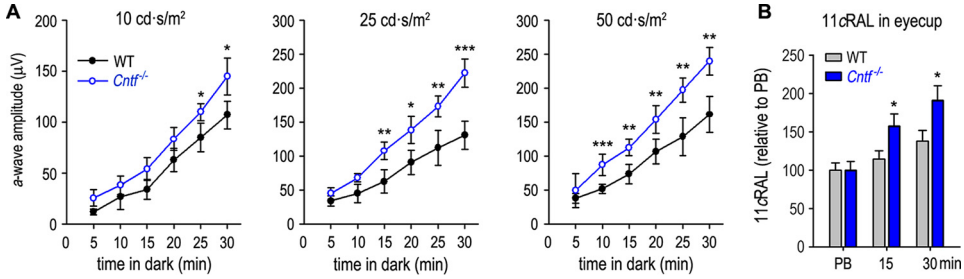

Figure 5. Faster recovery of rod light sensitivity in *Cntf*$^{-/-}$ mice. *A,* amplitudes of scotopic ERG *a*-waves elicited with the indicated flashes (10∼50 cd × s/m^2) in WT and *Cntf*$^{-/-}$ mice, which were kept in darkness for the indicated minutes after photobleaching the visual pigments. *Asterisks* indicate significant differences between WT and *Cntf*$^{-/-}$ mice (*, $p < 0.04$; **, $p \leq 0.009$; ***, $p \leq 0.003$); *error bars* show S.D. ($n = 6$). *B,* relative contents of 11*c*RAL in eyecups of mice under the indicated light conditions: immediately after PB of the visual pigment or kept in darkness for the indicated minutes after PB. *Error bars* show S.D. ($n = 4$).

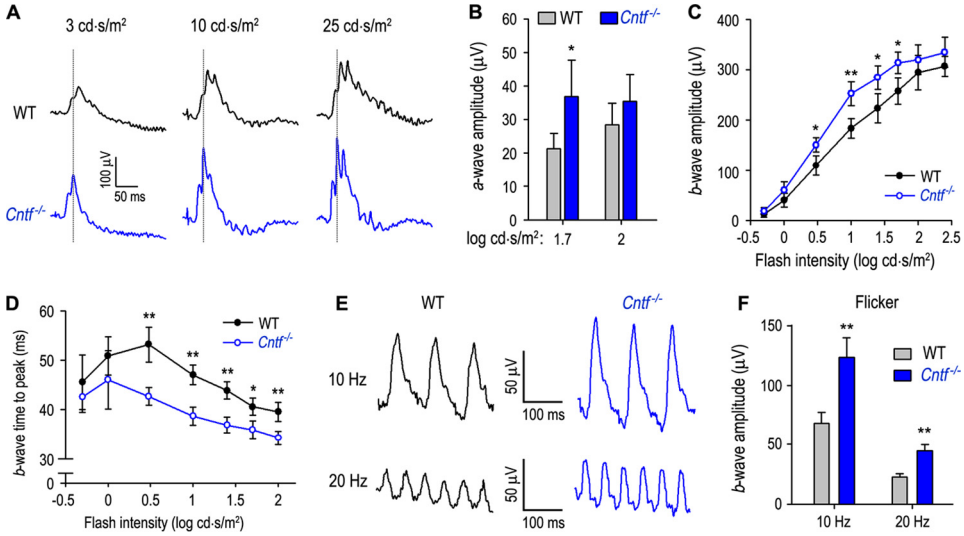

Figure 6. Hyper cone phototransduction in *Cntf*$^{-/-}$ mice. *A,* representative raw photopic ERG responses of WT and *Cntf*$^{-/-}$ mice to the indicated flashes under a rod saturating background light (32 cd/m^2). *B* and *C,* amplitudes of *a*-wave (*B*) and *b*-wave (*C*) in photopic ERG responses elicited with the indicated flash intensities in light (32 cd/m^2)-adapted WT and *Cntf*$^{-/-}$ mice. *Asterisks* indicate significant differences between WT and *Cntf*$^{-/-}$ mice (*, $p < 0.03$; **, $p \leq 0.001$); *error bars* show S.D. ($n = 7$). *D,* times from stimulus onset to photopic *b*-wave peaks of WT and *Cntf*$^{-/-}$ mouse cones. *E,* representative raw flicker ERG responses of WT and *Cntf*$^{-/-}$ mice to 10 cd × s/m^2 flashes with frequencies of 10 or 20 Hz on the rod saturating background light. *F,* amplitudes of *b*-wave in the flicker ERG responses of WT and *Cntf*$^{-/-}$ mice. *Error bars* show S.D. ($n = 5$, **, $p \leq 0.001$).

min), and then kept them in darkness for 5 days. Retinoid analysis showed that the contents of 11*c*RAL and the total retinoids were significantly reduced in the *Cntf*$^{-/-}$ eyes exposed to the intense light for 75 min, as compared with those in WT mice under that same light conditions (Fig. 7*A*). *Cntf*$^{-/-}$, but not WT, mice under that same light conditions displayed a significant reduction in rod visual function, as measured by scotopic ERG (Fig. 7*B*). Notably, both *a*- and *b*-wave amplitudes are markedly reduced in *Cntf*$^{-/-}$ mice (Fig. 7*B*). This reduction of rod visual function is associated with a dramatic decrease in rod OS length and contents of rhodopsin in the *Cntf*$^{-/-}$ retina (Fig. 7, *C* and *D*). Morphological analysis showed that 75 min exposure of 12,000 lux light caused a severe retinal degeneration in *Cntf*$^{-/-}$, but not WT, mice (Fig. 8, *B* and *C*). The superior ONL in *Cntf*$^{-/-}$ retina was reduced in thickness to 2–8 nuclei *versus* 9–10 nuclei in WT retina whereas the inferior ONL in the *Cntf*$^{-/-}$ retina was reduced to 4–8 nuclei *versus* 10–11 nuclei in WT retina (Fig. 8*D*).

Generally, cones are resistant to light-induced degeneration (45, 46). To know if CNTF deficiency increases susceptibility of cones to photodamage, we did immunohistochemistry for cones in WT and *Cntf*$^{-/-}$ mice exposed to the intense light for 75 min. Lengths of both S-cone and M-cone OSs are significantly shortened in *Cntf*$^{-/-}$ mice (Fig. 9, *B* and *C*). Consistent with these observations, immunoblot analysis showed that expression levels of S- and M-opsins were reduced at least 40% in the *Cntf*$^{-/-}$ retinas, as compared with those in WT retinas (Fig. 9, *D* and *E*).

Discussion

Phototransduction and the visual cycle are the most important functions in sensing and converting light signal into biochemical and electrical signals in the retina. Light sensitivities of both rod and cone visual pigments rely on their 11*c*RAL chromophore provided by the visual cycle. In this study, we showed that CNTF deficiency resulted in up-regulation of opsins and the visual cycle enzymes, leading to an increase in thickness of ONL, length of rod and cone OSs, and the rates of the 11*c*RAL regeneration. These molecular and morphological changes led to 1) hyper phototransduction of rods and cones, 2) faster recovery of rod light sensitivity, and 3) increase in susceptibility of rods and cones to photodamage in *Cntf*$^{-/-}$ mouse.

Up-regulation of opsins and the visual cycle enzymes (Figs. 1–3) are the most important primary phenotypes in the

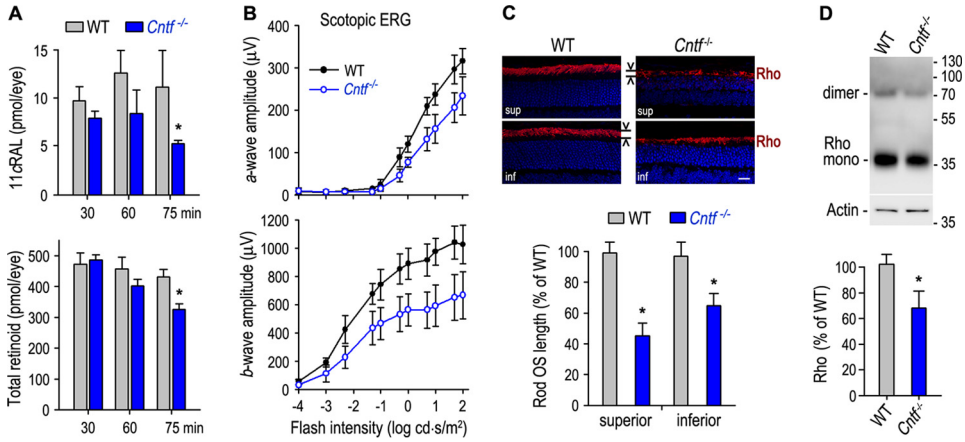

Figure 7. Reduction of retinoids, rod visual function, and rhodopsin contents in *Cntf*$^{-/-}$ mice exposed to intense light. *A,* contents of 11*c*RAL and total retinoids in the eyecups of WT and *Cntf*$^{-/-}$ mice kept in darkness for 5 days after exposing to 12,000 lux light for the indicated time. All *asterisks* indicate a significant difference between WT and *Cntf*$^{-/-}$ mice ($p < 0.02$); *error bars* show S.D. ($n = 4$). *B*, amplitudes of *a*-wave (*upper panel*) and *b*-wave (*bottom panel*) in scotopic ERG responses of WT and *Cntf*$^{-/-}$ mice to the indicated flashes. *Error bars* show S.D. ($n = 5$). All data shown in *B–D* are from mice kept in darkness for 5 days after exposing to 12,000 lux light for 75 min. *C*, immunohistochemistry for Rho in retinal sections of WT and *Cntf*$^{-/-}$ mice. Histograms show relative lengths of Rho-positive OS in WT and *Cntf*$^{-/-}$ retinal sections. *Scale bar* denotes 20 μm. *D*, immunoblot analysis of Rho in WT and *Cntf*$^{-/-}$ retinas. Histogram shows immunoblot intensities of Rho from *Cntf*$^{-/-}$ retinas relative to Rho intensity in WT retinas.

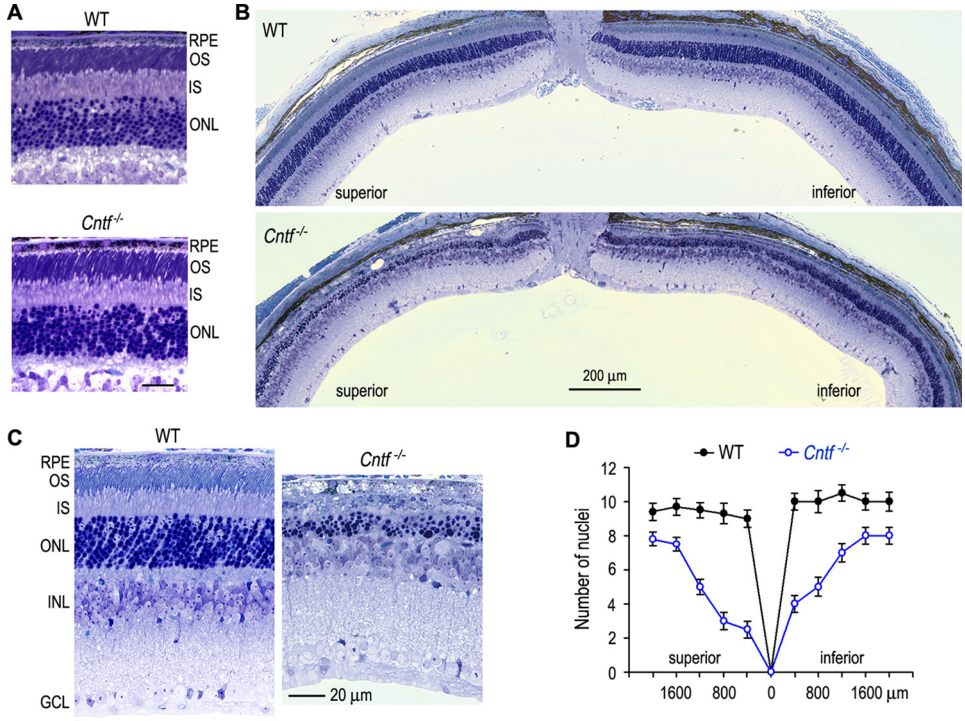

Figure 8. Retinal photodamage in *Cntf*$^{-/-}$ mice. *A,* light microscopic images of WT and *Cntf*$^{-/-}$ superior retinas before photodamage. *Scale bar* denotes 20 μm. *B*, light microscopy showing severe retinal degeneration in *Cntf*$^{-/-}$, but not WT, mice kept in darkness for 5 days after exposing to 12,000 lux light for 75 min. *C*, higher magnification images of the superior retinas of WT and *Cntf*$^{-/-}$ mice exposed to the intense light. *D*, thickness of the retinal outer nuclear layers in WT and *Cntf*$^{-/-}$ mice in *B*. *Numbers* on the *x*-axis indicate distance from optic nerve head. *Error bars* show S.D. ($n = 4$).

Cntf$^{-/-}$ visual system. CNTF might down-regulate these proteins through the heterotrimeric receptor complex (17), which can activate at least three distinct downstream pathways: Jak-STAT3, Ras-MAPK, and PI3K-AKT pathways (22, 47). The Jak-STAT3 pathway is the most studied pathway in CNTF/LIF signaling. Exogenous LIF activated STAT3 in mouse photoreceptors (48) and down-regulated rhodopsin (49), whereas CNTF did not activate STAT3 in any photoreceptors but down-regulated rhodopsin (23). CNTF might down-regulate rhodopsin by acting on Muller cells (23) or through the Ras-MAPK and/or PI3K-AKT pathways in rods.

Opsin up-regulation was accompanied by morphological changes in the *Cntf*$^{-/-}$ retina. The ONL thickness and lengths of rod and cone OSs were increased in *Cntf*$^{-/-}$ mice. The increase in the ONL thickness might be associated with the decrease in programed cell death in the ONL of postnatal *Cntf*$^{-/-}$ mice (Fig. 1). CNTF has been shown to promote programed death of postmitotic rod precursor cells; and blocking the CNTF/LIF pathway reduced cell death during mouse retinal development, resulting a thicker ONL (50).

CNTF deficiency also resulted in an increase in lengths of both rod and cone OSs. This observation is consistent with

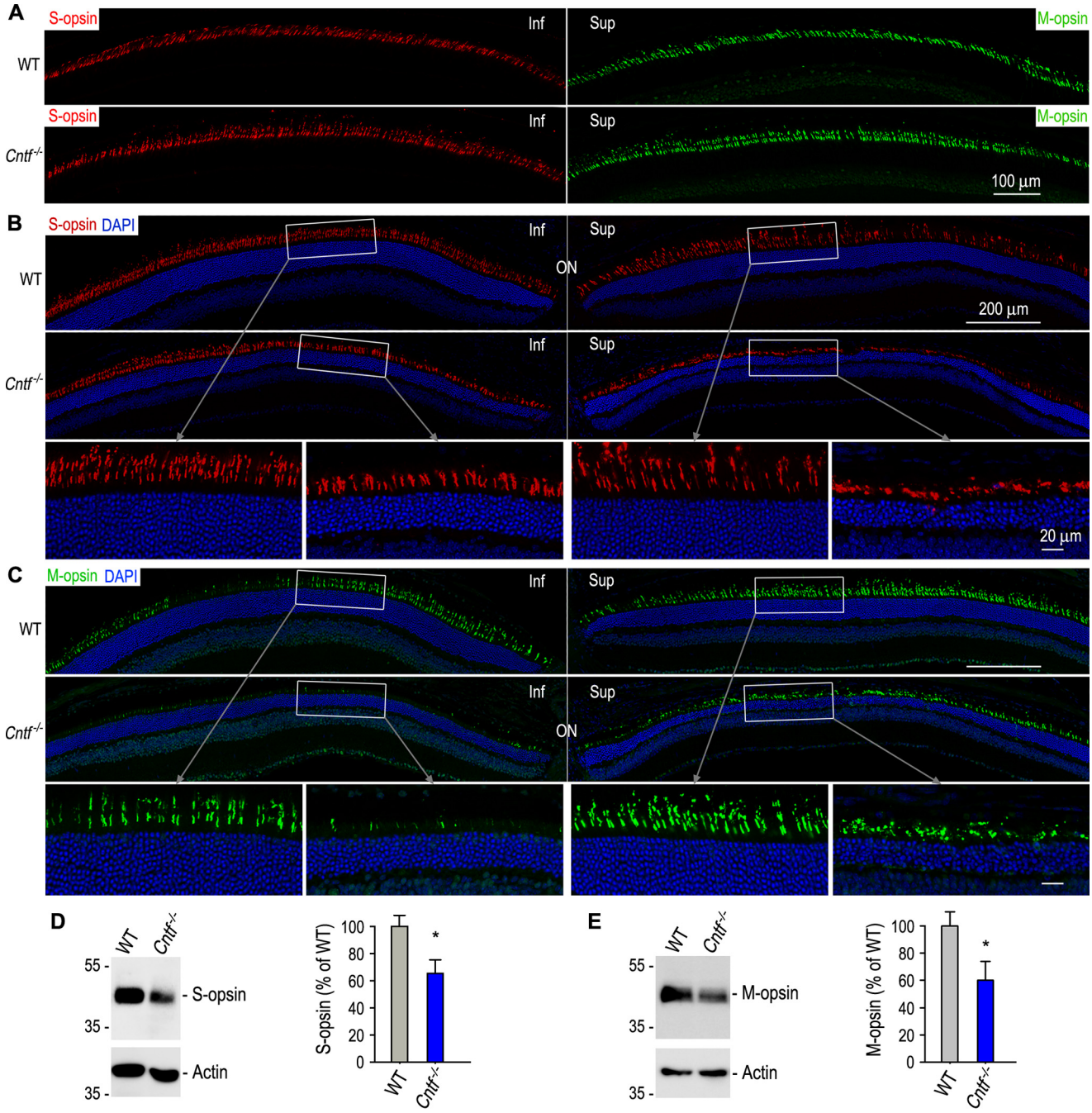

Figure 9. Light-induced degeneration of cones in *Cntf*$^{-/-}$ mice. *A*, immunohistochemistry showing cone opsin-positive OS in WT and *Cntf*$^{-/-}$ mice before photodamage. *B* and *C*, immunohistochemistry for S-opsin (*B*) or M-opsin (*C*) in retinal sections of WT and *Cntf*$^{-/-}$ mice kept in darkness for 5 days after exposing to 12,000 lux for 75 min. Nuclei were counterstained with DAPI (*blue*). The areas of the rectangles are shown in the higher magnification images (*bottom panels*). *Inf*, inferior; *sup*, superior; *ON*, optic nerve. All data shown in this figure are from mice exposed to 12,000 lux light for 75 min. *D* and *E*, immunoblot analysis of S-opsin (*D*) or M-opsin (*E*) in WT and *Cntf*$^{-/-}$ retinas. Actin was detected as sample loading control. Histograms show relative immunoblot intensities of S-opsin (*D*) or M-opsin (*E*) in WT *versus* *Cntf*$^{-/-}$ retinas. *Asterisks* indicate significant differences between WT and *Cntf*$^{-/-}$ mice ($p < 0.02$); *error bars* show S.D. ($n = 3$).

three previous studies: 1) CNTF induced a reversible rod OS shortening in WT rat (23), 2) CNTF reduced cone OS length in the *rds* mouse (51), and 3) transgenic LIF inhibited rod and cone OS maturation and/or elongation (52). In a rat line carrying a rhodopsin mutation, however, CNTF promoted regeneration of cone OS (32). The different effects of CNTF on cone OS morphology may depend on the presence or absence of strong inflammatory stimulation (53), which produce numerous signaling proteins in the retina (54).

11*c*RAL bound with opsins functions as a molecular switch for initiating phototransduction in response to light stimuli. Light-mediated isomerization of 11*c*RAL to all-*trans*-retinal induces opsin activation and phototransduction. To restore light sensitivity to opsins that have lost 11*c*RAL, 11*c*RAL must be regenerated and recombined with apo-opsins. RPE65 and LRAT are critical enzymes in the visual cycle that generates 11*c*RAL. We found that the synthesis rate of 11-*cis*-retinol in the *Cntf*$^{-/-}$ RPE was increased due to up-regulation of RPE65

and LRAT. RPE65 and LRAT might be up-regulated in part through the gp130-STAT3 pathway in the RPE (49). We further found that recovery of rod light sensitivity was accelerated due to an increase in 11*c*RAL synthesis in the *Cntf*$^{-/-}$ RPE (Fig. 5).

Increase in opsin expression and 11*c*RAL synthesis suggest that the *Cntf*$^{-/-}$ rods and cones contain more light-sensitive visual pigments. This might cause the enhanced responses of *Cntf*$^{-/-}$ rods and cones to light stimuli (Figs. 4–6). The hyper phototransduction led to greater hyperpolarization of rods and cones, reflected in elevation of *a*-wave amplitudes in both scotopic and photopic ERGs of *Cntf*$^{-/-}$ mice.

Although scotopic *a*-wave amplitudes were increased in *Cntf*$^{-/-}$ mice *b*-wave amplitudes, implicit times were similar to those in WT mice. In addition, expression levels of mGluR6 and PKCα in the *Cntf*$^{-/-}$ retina were also similar to those in WT retina. These results suggest that synaptic function between rod and rod ON-BC, which produce *b*-wave responses (55, 56), is not significantly changed or may be slightly reduced in *Cntf*$^{-/-}$ mice. Overexpression of CNTF or LIF has been shown to cause BC disorganization (51, 57). Exogenous CNTF has also been shown to promote BC differentiation (21, 51) through increasing Ath3 expression and pleiotrophin secretion (58, 59). These studies and the similar *b*-wave amplitudes in *Cntf*$^{-/-}$ and WT mice suggest that CNTF plays an important role in the development, differentiation, and function of rod ON-BCs.

Interestingly, cone *b*-wave amplitudes and implicit times in photopic ERG elicited with certain flash intensities were significantly higher or shorter in *Cntf*$^{-/-}$ mice *versus* WT mice. These results are consistent with the previous studies that show significant reduction of photopic *b*-waves in WT animals overexpressing CNTF (41, 42). Because *b*-waves of photopic and flicker ERGs are mainly from depolarizing cone ON-BCs (60, 61), our results suggest that the synaptic function between cone and cone ON-BC, as well as cone-induced depolarization of cone ON-BCs are enhanced in *Cntf*$^{-/-}$ mouse.

One of the pathological consequences of CNTF deficiency was retinal photodamage. *Cntf*$^{-/-}$ rods exhibited hyper susceptibility to light-induced degeneration. This phenotype is consistent with the well-known phenomenon: the rodent superior retina has much higher susceptibility to photodamage, as compared with the inferior retina. Length of photoreceptor OS in the superior retina is ~30% longer than that in the inferior retina (62). The longer OSs in the *Cntf*$^{-/-}$ and the rodent superior retinas may contain more rhodopsin, the primary mediator of retinal degeneration induced by light (9). Activated rhodopsin may increase the DNA-binding activity of the transcription factor AP-1 to promote light-induced apoptosis of photoreceptors (9, 63). In *Drosophila*, activated rhodopsin induced photoreceptor apoptosis by promoting clathrin-dependent endocytosis of rhodopsin-arrestin complexes (64).

It has been known that the higher expression level and activity of RPE65 cause an increase in susceptibility of retina to photodamage (10–12). Conversely, decrease in the visual cycle rate or RPE65 activity reduce retinal photodamage (65–67). RPE65 promotes retinal photodamage by facilitating the visual cycle that provides 11*c*RAL to generate light-sensitive visual pigments. Up-regulated RPE65 and LRAT have accelerated the synthesis rate of 11*c*RAL in the *Cntf*$^{-/-}$ mouse. This accelerated visual cycle plus increased expression of opsins resulted in an increase in the formation of light-sensitive visual pigment, therefore promoted retinal photodamage in *Cntf*$^{-/-}$ mice.

In general, cones are resistant to photodamage (45, 46). In this study, however, we observed that intense light caused a severe degeneration of both M- and S-cones in the *Cntf*$^{-/-}$ mouse. This result suggests that CNTF deficiency itself and increased formation of cone visual pigments contributed to cone photodamage in *Cntf*$^{-/-}$ mouse. In addition, increased visual cycle and phototransduction rates may result in elevation of oxidative stress in cones due to an increase in contents of 11*c*RAL and all-*trans*-retinal in the *Cntf*$^{-/-}$ cones. Retinaldehydes have been shown to play a critical role in retinal photooxidative damage (68–70). Cones are known to have high susceptibility to oxidative stress (71–74). Overexpression of NRF2, a master antioxidant transcription factor, effectively protected cones from degeneration in animal models of retinal degeneration (75). These studies and our results suggest that reduction of neuroprotective signals and increase in oxidative stress promoted light-induced cone degeneration in *Cntf*$^{-/-}$ mice. In summary, we identified CNTF as a critical signal that down-regulates rod and cone opsins, as well as RPE65 and LRAT, to suppress visual pigment over formation and retinal photodamage.

Experimental procedures

Animals

We crossed *Cntf*$^{-/-}$ mice (76) with WT 129S2/Sv mice (Charles River Laboratories), then intercrossed the heterozygous offspring to yield *Cntf*$^{-/-}$ mice homozygous for the Leu-450 allele of the *Rpe65* gene. The homologous *Cntf* knockout mutation and the Leu-450 alleles were confirmed by PCR and DNA sequencing, as described previously (12, 76). Except where noted, mice were maintained in 12 h cyclic light at ~30 lux. All animal experiments were performed on both sexes of WT and *Cntf*$^{-/-}$ mice at 3, 5, or 6 weeks of age in accordance with the Association for Research of Vision and Ophthalmology statement for the use of animals in ophthalmic and vision research and the protocols approved by the Institutional Animal Care and Use Committee for LSU Health Sciences Center.

Eyecup RPE, cell culture, and transfection

After removal of the anterior section and neural retina, the RPE in 3-week-old *Cntf*$^{-/-}$ mouse eyecups were maintained in DMEM/F-12 medium (Thermo Fisher Scientific Inc.) supplemented with 10% heat-inactivated fetal bovine serum (FBS) and antibiotics (77). The 293T-LC cells maintained in DMEM (Invitrogen) with 10% FBS (78) were transfected with pRK5 or pRK5-CNTF plasmid DNA using the PolyJet transfection reagent (SignaGen Laboratories). After transfection, the cells were maintained overnight in DMEM/F-12 medium containing 5% FBS. These media with or without CNTF were incubated with the eyecup RPE for 6 h. All cultures were maintained in an incubator containing 5% CO_2.

Immunoblot analysis

Protein samples in the Laemmli buffer containing 50 mM DTT were incubated for 10 min at 70 °C (or room temperature

for opsins), separated by SDS-PAGE in a 10, 12, or 4–12% gradient polyacrylamide gel, and transferred to an Immobilon-P membrane (MilliporeSigma). The membrane was incubated in blocking buffer, primary antibody, and horseradish peroxidase-conjugated secondary antibody against rabbit, mouse, or goat IgG. Antibodies against RPE65 (79), LRAT (80, 81), CNTF (Santa Cruz Biotechnology), Ezrin (ProteinTech), interphotoreceptor retinoid-binding protein (IRBP) (82), mGluR6 (GeneTex), PKCα, rhodopsin, CAR, M-opsin (MilliporeSigma), S-opsin (MilliporeSigma, Santa Cruz Biotechnology), or β-actin (MilliporeSigma) were used as the primary antibodies. Immunoblots were visualized with the enhanced ECL-Prime and quantified (82).

Immunohistochemistry

Retinal cryosections were prepared from the dorsal-ventral midline of mouse eye as described previously (83). Briefly, enucleated mouse eyeballs were fixed overnight with 4% paraformaldehyde in 0.1 M phosphate buffer (PB). After removing cornea and lens, eyecups were immersed in 15% sucrose in 0.1 M PB for 2 h, in 30% sucrose in 0.1 M PB for 2 h, and then in a 1:1 mixture of 30% sucrose and optimal cutting temperature (OCT) medium (Sakura Finetechnical) overnight at 4 °C. After embedding eyecups in OCT, 15-μm thick sections were cut on a Shandon Cryotome SME cryostat (Thermo Scientific). The sections were immunostained with the primary antibodies listed in the method of immunoblot analysis and secondary antibodies, as described previously (82). Nuclei were counterstained with DAPI (Sigma). Images were captured with a Zeiss LSM710 Meta confocal microscope with a ×20 objective lens or ×40 oil-immersion lens. Lengths of rod and cone OS as well as numbers of cells were measured using ImageJ software (National Institutes of Health).

TUNEL assay

This assay was performed using the *in situ* cell death detection kit (Roche Applied Science) following the manufacturer's protocol. Briefly, retinal cryosections washed with 0.1% sodium citrate in 0.1% Triton X-100, PBS were incubated with terminal deoxynucleotidyl transferase (TdT) and fluorescein-dUTP for 1 h at 37 °C. After rinsing three times in PBS containing 0.05% Tween 20, nuclei were counterstained with DAPI. Numbers of TUNEL-positive nuclear in the ONL-outer plexiform layer and in the inner nuclear layer-inner plexiform layer of whole retinal sections were counted separately using an Olympus BX61VS microscope equipped with a digital camera and VS-ASW FL software.

Quantitative RT-PCR

Total RNA was extracted from mouse retina or RPE using a PureLink RNA mini kit (Invitrogen), and was reverse-transcribed to cDNA using SuperScript III (Invitrogen). Quantitative PCR was performed on an iCylcer iQ^{TM} Real-Time PCR Detection System (Bio-Rad) using a two-step qRT-PCR kit with SYBR Green (Invitrogen) and primer sets specific for mouse RPE65, opsin, and 18S rRNA. Three mice of each genotype were analyzed and all samples were run in duplicates. Starting templates were normalized after determining 18S rRNA C_t values for each sample (84). Relative mRNA levels of RPE65 were determined from the ΔC_t values.

Electroretinography (ERG)

Overnight dark-adapted 6-week-old mice were anesthetized with an intraperitoneal injection of 100 mg/kg of ketamine and 10 mg/kg of xylazine. The pupils were dilated with 1% tropicamide. ERG was recorded from the corneal surface using a silver-silver chloride wire electrode referenced to a subcutaneous electrode in the mouth. A needle electrode in the tail served as the ground. A drop of 2.5% methylcellulose was placed on the cornea to ensure good electrical contact and to prevent corneal desiccation during the entire procedure. Single-flash ERG recordings were performed in a Ganzfield dome (Espion e2, Diagnosys LLC) under dark-adapted (scotopic) and light-adapted (photopic) conditions. For scotopic ERG, single flash stimuli were presented with various intensities, reaching from -4 log cd × s/m^2 to 2.5 log cd × s/m^2, in interstimulus intervals of 0.5∼2 min (depending on the stimulus intensity). Three to four responses were averaged for each step. For photopic ERG, animals were light adapted for 10 min by exposing to a white 32 cd/m^2 light, and ERG responses were obtained with white flashes (-0.3∼2.4 log cd × s/m^2) on the rod-saturating background light (32 cd/m^2). Five responses to 10-s interval flashes were averaged for each step. Intensity-response amplitude data were displayed on log-linear coordinates using SigmaPlot 11 software. Flicker ERG responses were recorded in light-adapted mice with flicker flashes on the rod-saturating background. The flicker stimuli had an intensity of 10 cd × s/m^2 with frequencies of 10 or 20 Hz.

Retinoid isomerase assay

RPE homogenates in 20 mM HEPES buffer (pH 7.4) containing protease inhibitor mixture were prepared from mouse eyecups without the neural retina. The homogenates were irradiated for 10 min on ice with 365-nm light from a Spectroline Model EN-140L UV light source to destroy endogenous retinoids. Each assay mixture contained 200 μg of cell homogenate, 10 μM all-*trans*-retinol, and 6% BSA. After incubating for 2 h in darkness at 37 °C, retinoids were extracted with hexane and analyzed by HPLC, as described below.

Analysis of retinoids

Retinoids in mouse ocular tissues or *in vitro* enzyme assays were extracted with hexane and analyzed by normal-phase HPLC (84). In brief, retinoids in hexane extractions were evaporated, dissolved in 100 μl of hexane, and separated on a silica column (Zorbax-Sil 5 μm, 250 × 4.6 mm, Agilent Technologies) by gradient (0.2–10% dioxane in hexane at 2.0 ml/min flow rate) or nongradient (10% dioxane in hexane at 1.0 ml/min flow rate) elution of mobile phase on an Agilent 1100 HPLC system equipped with a photodiode array detector (Agilent Technologies). Spectral data were acquired for all eluted peaks. Quantitation was performed by comparison of peak areas to calibration curves established with authentic retinoid standards.

Light microscopy

Mouse retinal sections were prepared as described previously (84). In brief, mice were fixed by intracardiac perfusion

with a mixture of 2% paraformaldehyde and 2.5% glutaraldehyde in 0.1 M PB (pH 7.4). Light cautery was applied at the superior pole of the cornea to mark the orientation before enucleation of the eyeball. A window was cut in the cornea, and the eye was immersed in primary fixative and rotated at room temperature for 2 h. The anterior segment was removed, and the remaining eyecup was refrigerated overnight in primary fixative. The eyecup was trimmed into temporal and nasal hemispheres and immersed in 1% osmium tetroxide in 0.1 M PB (pH 7.2) for 1 h. Following dehydration in a graded series of alcohols, the hemispheres were embedded in an Epon/Araldite mixture (5:3, v/v). Care was taken to orient the eyecups so that sections were obtained through the vertical meridian to ensure sampling of both the superior, green-sensitive cones and the inferior, blue-sensitive cones. Sections were cut at 1 μm and stained with 1% toluidine blue and 1% sodium borate, then photographed using a $\times$20 objective lens or a $\times$60 oil-immersion lens in the Olympus BX61VS microscope mentioned above. Except for whole retinal images, all images were obtained from retinal sections at a distance of 600 μm superior or inferior to the optic nerve.

Light-induced retinal degeneration

WT and *Cntf*$^{-/-}$ mice were dark-adapted for 3 days. After dilation of the pupils under dim red light (Kodak Wratten 1A), mice were exposed to 12,000 lux of white fluorescent light for 30, 60, and 75 min and then kept in darkness for 5 days. Retinoid contents, visual function, and retinal structures of these mice were analyzed as described above.

Statistical analysis

SigmaPlot Version 11 (Systat Software, Inc.) was used for statistical analyses. Data were expressed as the mean $\pm$ S.D. of three or more independent experiments indicated in the figure legends. Differences between WT and *Cntf*$^{-/-}$ mice were determined by single comparisons with an unpaired two-tailed Student's *t* test. The significance threshold was set at 0.05 for all statistical tests.

Author contributions—S. L. and M. J. conceptualization; S. L., K. S., W. C. G., and M. S. data curation; S. L., N. G. B., and M. J. formal analysis; S. L. and M. J. validation; S. L. and M. J. investigation; S. L. and W. C. G. visualization; S. L., K. S., and W. C. G. methodology; S. L. and M. J. writing-original draft; S. L., W. C. G., N. G. B., and M. J. writing-review and editing; M. S. and N. G. B. resources; M. S., N. G. B., and M. J. funding acquisition; N. G. B. and M. J. project administration; K. S. and M. S. writing-review.

Acknowledgments—We are grateful to Dr. Paul A. Sieving for some ERG data analysis and valuable advice on some animal experiments, and Drs. Dean Bok, Marcin Golczak, and Krzysztof Palczewski for the antibodies against IRBP or LRAT.

References

1. Burns, M. E., and Arshavsky, V. Y. (2005) Beyond counting photons: trials and trends in vertebrate visual transduction. *Neuron* **48,** 387–401 CrossRef Medline
2. Palczewski, K. (2012) Chemistry and biology of vision. *J. Biol. Chem.* **287,** 1612–1619 CrossRef Medline
3. Jin, M., Li, S., Moghrabi, W. N., Sun, H., and Travis, G. H. (2005) Rpe65 is the retinoid isomerase in bovine retinal pigment epithelium. *Cell* **122,** 449–459 CrossRef Medline
4. Moiseyev, G., Chen, Y., Takahashi, Y., Wu, B. X., and Ma, J. X. (2005) RPE65 is the isomerohydrolase in the retinoid visual cycle. *Proc. Natl. Acad. Sci. U.S.A.* **102,** 12413–12418 CrossRef Medline
5. Redmond, T. M., Poliakov, E., Yu, S., Tsai, J. Y., Lu, Z., and Gentleman, S. (2005) Mutation of key residues of RPE65 abolishes its enzymatic role as isomerohydrolase in the visual cycle. *Proc. Natl. Acad. Sci. U.S.A.* **102,** 13658–13663 CrossRef Medline
6. Ruiz, A., Winston, A., Lim, Y. H., Gilbert, B. A., Rando, R. R., and Bok, D. (1999) Molecular and biochemical characterization of lecithin retinol acyltransferase. *J. Biol. Chem.* **274,** 3834–3841 CrossRef Medline
7. Kaschula, C. H., Jin, M. H., Desmond-Smith, N. S., and Travis, G. H. (2006) Acyl CoA:retinol acyltransferase (ARAT) activity is present in bovine retinal pigment epithelium. *Exp. Eye Res.* **82,** 111–121 CrossRef Medline
8. Kaylor, J. J., Radu, R. A., Bischoff, N., Makshanoff, J., Hu, J., Lloyd, M., Eddington, S., Bianconi, T., Bok, D., and Travis, G. H. (2015) Diacylglycerol *o*-acyltransferase type-1 synthesizes retinyl esters in the retina and retinal pigment epithelium. *PLoS ONE* **10,** e0125921 CrossRef Medline
9. Grimm, C., Wenzel, A., Hafezi, F., Yu, S., Redmond, T. M., and Remé, C. E. (2000) Protection of Rpe65-deficient mice identifies rhodopsin as a mediator of light-induced retinal degeneration. *Nat. Genet.* **25,** 63–66 CrossRef Medline
10. Danciger, M., Matthes, M. T., Yasamura, D., Akhmedov, N. B., Rickabaugh, T., Gentleman, S., Redmond, T. M., La Vail, M. M., and Farber, D. B. (2000) A QTL on distal chromosome 3 that influences the severity of light-induced damage to mouse photoreceptors. *Mamm. Genome* **11,** 422–427 CrossRef Medline
11. Wenzel, A., Reme, C. E., Williams, T. P., Hafezi, F., and Grimm, C. (2001) The Rpe65 Leu450Met variation increases retinal resistance against light-induced degeneration by slowing rhodopsin regeneration. *J. Neurosci.* **21,** 53–58 CrossRef Medline
12. Li, S., Lee, J., Zhou, Y., Gordon, W. C., Hill, J. M., Bazan, N. G., Miner, J. H., and Jin, M. (2013) Fatty acid transport protein 4 (FATP4) prevents light-induced degeneration of cone and rod photoreceptors by inhibiting RPE65 isomerase. *J. Neurosci.* **33,** 3178–3189 CrossRef Medline
13. Ju, W. K., Lee, M. Y., Hofmann, H. D., Kirsch, M., and Chun, M. H. (1999) Expression of CNTF in Muller cells of the rat retina after pressure-induced ischemia. *Neuroreport* **10,** 419–422 CrossRef Medline
14. Li, R., Wen, R., Banzon, T., Maminishkis, A., and Miller, S. S. (2011) CNTF mediates neurotrophic factor secretion and fluid absorption in human retinal pigment epithelium. *PLoS ONE* **6,** e23148 CrossRef Medline
15. Walsh, N., Valter, K., and Stone, J. (2001) Cellular and subcellular patterns of expression of bFGF and CNTF in the normal and light stressed adult rat retina. *Exp. Eye. Res.* **72,** 495–501 CrossRef Medline
16. Hollyfield, J. G. (1999) Hyaluronan and the functional organization of the interphotoreceptor matrix. *Invest. Ophthalmol. Vis. Sci.* **40,** 2767–2769 Medline
17. Wen, R., Tao, W., Li, Y., and Sieving, P. A. (2012) CNTF and retina. *Prog. Retin. Eye Res.* **31,** 136–151 CrossRef Medline
18. Beltran, W. A., Zhang, Q., Kijas, J. W., Gu, D., Rohrer, H., Jordan, J. A., and Aguirre, G. D. (2003) Cloning, mapping, and retinal expression of the canine ciliary neurotrophic factor receptor α (CNTFRα). *Invest. Ophthalmol. Vis. Sci.* **44,** 3642–3649 CrossRef Medline
19. Rhee, K. D., and Yang, X. J. (2003) Expression of cytokine signal transduction components in the postnatal mouse retina. *Mol. Vis.* **9,** 715–722 Medline
20. Beltran, W. A., Rohrer, H., and Aguirre, G. D. (2005) Immunolocalization of ciliary neurotrophic factor receptor α (CNTFRα) in mammalian photoreceptor cells. *Mol. Vis.* **11,** 232–244 Medline
21. Ezzeddine, Z. D., Yang, X., DeChiara, T., Yancopoulos, G., and Cepko, C. L. (1997) Postmitotic cells fated to become rod photoreceptors can be respecified by CNTF treatment of the retina. *Development* **124,** 1055–1067 Medline
22. Rhee, K. D., Goureau, O., Chen, S., and Yang, X. J. (2004) Cytokine-induced activation of signal transducer and activator of transcription in

photoreceptor precursors regulates rod differentiation in the developing mouse retina. *J. Neurosci.* **24,** 9779–9788 CrossRef Medline
23. Wen, R., Song, Y., Kjellstrom, S., Tanikawa, A., Liu, Y., Li, Y., Zhao, L., Bush, R. A., Laties, A. M., and Sieving, P. A. (2006) Regulation of rod phototransduction machinery by ciliary neurotrophic factor. *J. Neurosci.* **26,** 13523–13530 CrossRef Medline
24. Fuhrmann, S., Kirsch, M., and Hofmann, H. D. (1995) Ciliary neurotrophic factor promotes chick photoreceptor development *in vitro*. *Development* **121,** 2695–2706 Medline
25. Xie, H. Q., and Adler, R. (2000) Green cone opsin and rhodopsin regulation by CNTF and staurosporine in cultured chick photoreceptors. *Invest. Ophthalmol. Vis. Sci.* **41,** 4317–4323 Medline
26. Gupta, S. K., Jollimore, C. A., McLaren, M. J., Inana, G., and Kelly, M. E. (1997) Mammalian retinal pigment epithelial cells in vitro respond to the neurokines ciliary neurotrophic factor and leukemia inhibitory factor. *Biochem. Cell Biol.* **75,** 119–125 CrossRef Medline
27. LaVail, M. M., Unoki, K., Yasumura, D., Matthes, M. T., Yancopoulos, G. D., and Steinberg, R. H. (1992) Multiple growth factors, cytokines, and neurotrophins rescue photoreceptors from the damaging effects of constant light. *Proc. Natl. Acad. Sci. U.S.A.* **89,** 11249–11253 CrossRef Medline
28. Liang, F. Q., Dejneka, N. S., Cohen, D. R., Krasnoperova, N. V., Lem, J., Maguire, A. M., Dudus, L., Fisher, K. J., and Bennett, J. (2001) AAV-mediated delivery of ciliary neurotrophic factor prolongs photoreceptor survival in the rhodopsin knockout mouse. *Mol. Ther.* **3,** 241–248 CrossRef Medline
29. Bok, D., Yasumura, D., Matthes, M. T., Ruiz, A., Duncan, J. L., Chappelow, A. V., Zolutukhin, S., Hauswirth, W., and LaVail, M. M. (2002) Effects of adeno-associated virus-vectored ciliary neurotrophic factor on retinal structure and function in mice with a P216L rds/peripherin mutation. *Exp. Eye Res.* **74,** 719–735 CrossRef Medline
30. Tao, W., Wen, R., Goddard, M. B., Sherman, S. D., O'Rourke, P. J., Stabila, P. F., Bell, W. J., Dean, B. J., Kauper, K. A., Budz, V. A., Tsiaras, W. G., Acland, G. M., Pearce-Kelling, S., Laties, A. M., and Aguirre, G. D. (2002) Encapsulated cell-based delivery of CNTF reduces photoreceptor degeneration in animal models of retinitis pigmentosa. *Invest. Ophthalmol. Vis. Sci.* **43,** 3292–3298 Medline
31. Rhee, K. D., Nusinowitz, S., Chao, K., Yu, F., Bok, D., and Yang, X. J. (2013) CNTF-mediated protection of photoreceptors requires initial activation of the cytokine receptor gp130 in Muller glial cells. *Proc. Natl. Acad. Sci. U.S.A.* **110,** E4520–4529 CrossRef Medline
32. Li, Y., Tao, W., Luo, L., Huang, D., Kauper, K., Stabila, P., Lavail, M. M., Laties, A. M., and Wen, R. (2010) CNTF induces regeneration of cone outer segments in a rat model of retinal degeneration. *PLoS ONE* **5,** e9495 CrossRef Medline
33. Sieving, P. A., Caruso, R. C., Tao, W., Coleman, H. R., Thompson, D. J., Fullmer, K. R., and Bush, R. A. (2006) Ciliary neurotrophic factor (CNTF) for human retinal degeneration: phase I trial of CNTF delivered by encapsulated cell intraocular implants. *Proc. Natl. Acad. Sci. U.S.A.* **103,** 3896–3901 CrossRef Medline
34. Talcott, K. E., Ratnam, K., Sundquist, S. M., Lucero, A. S., Lujan, B. J., Tao, W., Porco, T. C., Roorda, A., and Duncan, J. L. (2011) Longitudinal study of cone photoreceptors during retinal degeneration and in response to ciliary neurotrophic factor treatment. *Invest. Ophthalmol. Vis. Sci.* **52,** 2219–2226 CrossRef Medline
35. Zhang, K., Hopkins, J. J., Heier, J. S., Birch, D. G., Halperin, L. S., Albini, T. A., Brown, D. M., Jaffe, G. J., Tao, W., and Williams, G. A. (2011) Ciliary neurotrophic factor delivered by encapsulated cell intraocular implants for treatment of geographic atrophy in age-related macular degeneration. *Proc. Natl. Acad. Sci. U.S.A.* **108,** 6241–6245 CrossRef Medline
36. Beltran, W. A., Wen, R., Acland, G. M., and Aguirre, G. D. (2007) Intravitreal injection of ciliary neurotrophic factor (CNTF) causes peripheral remodeling and does not prevent photoreceptor loss in canine RPGR mutant retina. *Exp. Eye Res.* **84,** 753–771 CrossRef Medline
37. Birch, D. G., Weleber, R. G., Duncan, J. L., Jaffe, G. J., Tao, W., and Ciliary Neurotrophic Factor Retinitis Pigmentosa Study Groups (2013) Randomized trial of ciliary neurotrophic factor delivered by encapsulated cell intraocular implants for retinitis pigmentosa. *Am. J. Ophthalmol.* **156,** 283–292 CrossRef Medline
38. Birch, D. G., Bennett, L. D., Duncan, J. L., Weleber, R. G., and Pennesi, M. E. (2016) Long-term follow-up of patients with retinitis pigmentosa receiving intraocular ciliary neurotrophic factor implants. *Am. J. Ophthalmol* **170,** 10–14 CrossRef Medline
39. Liang, F. Q., Aleman, T. S., Dejneka, N. S., Dudus, L., Fisher, K. J., Maguire, A. M., Jacobson, S. G., and Bennett, J. (2001) Long-term protection of retinal structure but not function using RAAV.CNTF in animal models of retinitis pigmentosa. *Mol. Ther.* **4,** 461–472 CrossRef Medline
40. Schlichtenbrede, F. C., MacNeil, A., Bainbridge, J. W., Tschernutter, M., Thrasher, A. J., Smith, A. J., and Ali, R. R. (2003) Intraocular gene delivery of ciliary neurotrophic factor results in significant loss of retinal function in normal mice and in the Prph2Rd2/Rd2 model of retinal degeneration. *Gene Ther.* **10,** 523–527 CrossRef Medline
41. Bush, R. A., Lei, B., Tao, W., Raz, D., Chan, C. C., Cox, T. A., Santos-Muffley, M., and Sieving, P. A. (2004) Encapsulated cell-based intraocular delivery of ciliary neurotrophic factor in normal rabbit: dose-dependent effects on ERG and retinal histology. *Invest. Ophthalmol. Vis. Sci.* **45,** 2420–2430 CrossRef Medline
42. McGill, T. J., Prusky, G. T., Douglas, R. M., Yasumura, D., Matthes, M. T., Nune, G., Donohue-Rolfe, K., Yang, H., Niculescu, D., Hauswirth, W. W., Girman, S. V., Lund, R. D., Duncan, J. L., and LaVail, M. M. (2007) Intraocular CNTF reduces vision in normal rats in a dose-dependent manner. *Invest. Ophthalmol. Vis. Sci.* **48,** 5756–5766 CrossRef Medline
43. Xue, W., Cojocaru, R. I., Dudley, V. J., Brooks, M., Swaroop, A., and Sarthy, V. P. (2011) Ciliary neurotrophic factor induces genes associated with inflammation and gliosis in the retina: a gene profiling study of flow-sorted, Muller cells. *PLoS ONE* **6,** e20326 CrossRef Medline
44. Zhu, X., Brown, B., Li, A., Mears, A. J., Swaroop, A., and Craft, C. M. (2003) GRK1-dependent phosphorylation of S and M opsins and their binding to cone arrestin during cone phototransduction in the mouse retina. *J. Neurosci.* **23,** 6152–6160 CrossRef Medline
45. Kunchithapautham, K., Coughlin, B., Lemasters, J. J., and Rohrer, B. (2011) Differential effects of rapamycin on rods and cones during light-induced stress in albino mice. *Invest. Ophthalmol. Vis. Sci.* **52,** 2967–2975 CrossRef Medline
46. Okano, K., Maeda, A., Chen, Y., Chauhan, V., Tang, J., Palczewska, G., Sakai, T., Tsuneoka, H., Palczewski, K., and Maeda, T. (2012) Retinal cone and rod photoreceptor cells exhibit differential susceptibility to light-induced damage. *J. Neurochem.* **121,** 146–156 CrossRef Medline
47. Kassen, S. C., Thummel, R., Campochiaro, L. A., Harding, M. J., Bennett, N. A., and Hyde, D. R. (2009) CNTF induces photoreceptor neuroprotection and Muller glial cell proliferation through two different signaling pathways in the adult zebrafish retina. *Exp. Eye Res.* **88,** 1051–1064 CrossRef Medline
48. Ueki, Y., Wang, J., Chollangi, S., and Ash, J. D. (2008) STAT3 activation in photoreceptors by leukemia inhibitory factor is associated with protection from light damage. *J. Neurochem.* **105,** 784–796 CrossRef Medline
49. Chucair-Elliott, A. J., Elliott, M. H., Wang, J., Moiseyev, G. P., Ma, J. X., Politi, L. E., Rotstein, N. P., Akira, S., Uematsu, S., and Ash, J. D. (2012) Leukemia inhibitory factor coordinates the down-regulation of the visual cycle in the retina and retinal-pigmented epithelium. *J. Biol. Chem.* **287,** 24092–24102 CrossRef Medline
50. Elliott, J., Cayouette, M., and Gravel, C. (2006) The CNTF/LIF signaling pathway regulates developmental programmed cell death and differentiation of rod precursor cells in the mouse retina *in vivo*. *Dev. Biol.* **300,** 583–598 CrossRef Medline
51. Rhee, K. D., Ruiz, A., Duncan, J. L., Hauswirth, W. W., Lavail, M. M., Bok, D., and Yang, X. J. (2007) Molecular and cellular alterations induced by sustained expression of ciliary neurotrophic factor in a mouse model of retinitis pigmentosa. *Invest. Ophthalmol. Vis. Sci.* **48,** 1389–1400 CrossRef Medline
52. Graham, D. R., Overbeek, P. A., and Ash, J. D. (2005) Leukemia inhibitory factor blocks expression of Crx and Nrl transcription factors to inhibit photoreceptor differentiation. *Invest. Ophthalmol. Vis. Sci.* **46,** 2601–2610 CrossRef Medline

53. Fischer, D. (2017) Hyper-IL-6: a potent and efficacious stimulator of RGC regeneration. *Eye (Lond)* **31,** 173–178 Medline
54. Wen, R., Song, Y., Cheng, T., Matthes, M. T., Yasumura, D., LaVail, M. M., and Steinberg, R. H. (1995) Injury-induced upregulation of bFGF and CNTF mRNAS in the rat retina. *J. Neurosci.* **15,** 7377–7385 CrossRef Medline
55. Stockton, R. A., and Slaughter, M. M. (1989) B-wave of the electroretinogram: a reflection of ON bipolar cell activity. *J. Gen. Physiol.* **93,** 101–122 CrossRef Medline
56. Hood, D. C., and Birch, D. G. (1996) Beta wave of the scotopic (rod) electroretinogram as a measure of the activity of human on-bipolar cells. *J. Opt. Soc. Am. A Opt. Image Sci. Vis.* **13,** 623–633 CrossRef Medline
57. Sherry, D. M., Mitchell, R., Li, H., Graham, D. R., and Ash, J. D. (2005) Leukemia inhibitory factor inhibits neuronal development and disrupts synaptic organization in the mouse retina. *J. Neurosci. Res.* **82,** 316–332 CrossRef Medline
58. Bhattacharya, S., Dooley, C., Soto, F., Madson, J., Das, A. V., and Ahmad, I. (2004) Involvement of Ath3 in CNTF-mediated differentiation of the late retinal progenitors. *Mol. Cell Neurosci.* **27,** 32–43 CrossRef Medline
59. Roger, J., Brajeul, V., Thomasseau, S., Hienola, A., Sahel, J. A., Guillonneau, X., and Goureau, O. (2006) Involvement of Pleiotrophin in CNTF-mediated differentiation of the late retinal progenitor cells. *Dev. Biol.* **298,** 527–539 CrossRef Medline
60. Lei, B., Bush, R. A., Milam, A. H., and Sieving, P. A. (2000) Human melanoma-associated retinopathy (MAR) antibodies alter the retinal ON-response of the monkey ERG *in vivo*. *Invest. Ophthalmol. Vis. Sci.* **41,** 262–266 Medline
61. Kondo, M., and Sieving, P. A. (2001) Primate photopic sine-wave flicker ERG: vector modeling analysis of component origins using glutamate analogs. *Invest. Ophthalmol. Vis. Sci.* **42,** 305–312 Medline
62. Battelle, B. A., and LaVail, M. M. (1978) Rhodopsin content and rod outer segment length in albino rat eyes: modification by dark adaptation. *Exp. Eye Res.* **26,** 487–497 CrossRef Medline
63. Hafezi, F., Steinbach, J. P., Marti, A., Munz, K., Wang, Z. Q., Wagner, E. F., Aguzzi, A., and Remé, C. E. (1997) The absence of c-fos prevents light-induced apoptotic cell death of photoreceptors in retinal degeneration *in vivo*. *Nat. Med.* **3,** 346–349 CrossRef Medline
64. Kiselev, A., Socolich, M., Vinós, J., Hardy, R. W., Zuker, C. S., and Ranganathan, R. (2000) A molecular pathway for light-dependent photoreceptor apoptosis in *Drosophila*. *Neuron* **28,** 139–152 CrossRef Medline
65. Sieving, P. A., Chaudhry, P., Kondo, M., Provenzano, M., Wu, D., Carlson, T. J., Bush, R. A., and Thompson, D. A. (2001) Inhibition of the visual cycle *in vivo* by 13-cis retinoic acid protects from light damage and provides a mechanism for night blindness in isotretinoin therapy. *Proc. Natl. Acad. Sci. U.S.A.* **98,** 1835–1840 CrossRef Medline
66. Maeda, A., Maeda, T., Golczak, M., Imanishi, Y., Leahy, P., Kubota, R., and Palczewski, K. (2006) Effects of potent inhibitors of the retinoid cycle on visual function and photoreceptor protection from light damage in mice. *Mol. Pharmacol.* **70,** 1220–1229 CrossRef Medline
67. Lopes, V. S., Gibbs, D., Libby, R. T., Aleman, T. S., Welch, D. L., Lillo, C., Jacobson, S. G., Radu, R. A., Steel, K. P., and Williams, D. S. (2011) The Usher 1B protein, MYO7A, is required for normal localization and function of the visual retinoid cycle enzyme, RPE65. *Hum. Mol. Genet.* **20,** 2560–2570 CrossRef Medline
68. Maeda, A., Maeda, T., Golczak, M., Chou, S., Desai, A., Hoppel, C. L., Matsuyama, S., and Palczewski, K. (2009) Involvement of all-*trans*-retinal in acute light-induced retinopathy of mice. *J. Biol. Chem.* **284,** 15173–15183 CrossRef Medline
69. Chen, Y., Okano, K., Maeda, T., Chauhan, V., Golczak, M., Maeda, A., and Palczewski, K. (2012) Mechanism of all-*trans*-retinal toxicity with implications for stargardt disease and age-related macular degeneration. *J. Biol. Chem.* **287,** 5059–5069 CrossRef Medline
70. Lee, M., Li, S., Sato, K., and Jin, M. (2016) Interphotoreceptor retinoid-binding protein mitigates cellular oxidative stress and mitochondrial dysfunction induced by all-*trans*-retinal. *Invest. Ophthalmol. Vis. Sci.* **57,** 1553–1562 CrossRef Medline
71. Shen, J., Yang, X., Dong, A., Petters, R. M., Peng, Y. W., Wong, F., and Campochiaro, P. A. (2005) Oxidative damage is a potential cause of cone cell death in retinitis pigmentosa. *J. Cell. Physiol.* **203,** 457–464 CrossRef Medline
72. Komeima, K., Usui, S., Shen, J., Rogers, B. S., and Campochiaro, P. A. (2008) Blockade of neuronal nitric oxide synthase reduces cone cell death in a model of retinitis pigmentosa. *Free Radic. Biol. Med.* **45,** 905–912 CrossRef Medline
73. Usui, S., Oveson, B. C., Lee, S. Y., Jo, Y. J., Yoshida, T., Miki, A., Miki, K., Iwase, T., Lu, L., and Campochiaro, P. A. (2009) NADPH oxidase plays a central role in cone cell death in retinitis pigmentosa. *J. Neurochem.* **110,** 1028–1037 CrossRef Medline
74. Campochiaro, P. A., and Mir, T. A. (2018) The mechanism of cone cell death in retinitis pigmentosa. *Prog. Retin. Eye Res.* **62,** 24–37 CrossRef Medline
75. Xiong, W., MacColl Garfinkel, A. E., Li, Y., Benowitz, L. I., and Cepko, C. L. (2015) NRF2 promotes neuronal survival in neurodegeneration and acute nerve damage. *J. Clin. Invest.* **125,** 1433–1445 CrossRef Medline
76. Masu, Y., Wolf, E., Holtmann, B., Sendtner, M., Brem, G., and Thoenen, H. (1993) Disruption of the *CNTF* gene results in motor neuron degeneration. *Nature* **365,** 27–32 CrossRef Medline
77. Li, S., Samardzija, M., Yang, Z., Grimm, C., and Jin, M. (2016) Pharmacological amelioration of cone survival and vision in a mouse model for Leber congenital amaurosis. *J. Neurosci.* **36,** 5808–5819 CrossRef Medline
78. Li, S., Izumi, T., Hu, J., Jin, H. H., Siddiqui, A. A., Jacobson, S. G., Bok, D., and Jin, M. (2014) Rescue of enzymatic function for disease-associated RPE65 proteins containing various missense mutations in non-active sites. *J. Biol. Chem.* **289,** 18943–18956 CrossRef Medline
79. Jin, M., Yuan, Q., Li, S., and Travis, G. H. (2007) Role of LRAT on the retinoid isomerase activity and membrane association of Rpe65. *J. Biol. Chem.* **282,** 20915–20924 CrossRef Medline
80. Batten, M. L., Imanishi, Y., Maeda, T., Tu, D. C., Moise, A. R., Bronson, D., Possin, D., Van Gelder, R. N., Baehr, W., and Palczewski, K. (2004) Lecithin-retinol acyltransferase is essential for accumulation of all-*trans*-retinyl esters in the eye and in the liver. *J. Biol. Chem.* **279,** 10422–10432 CrossRef Medline
81. Golczak, M., Kuksa, V., Maeda, T., Moise, A. R., and Palczewski, K. (2005) Positively charged retinoids are potent and selective inhibitors of the trans-cis isomerization in the retinoid (visual) cycle. *Proc. Natl. Acad. Sci. U.S.A.* **102,** 8162–8167 CrossRef Medline
82. Li, S., Yang, Z., Hu, J., Gordon, W. C., Bazan, N. G., Haas, A. L., Bok, D., and Jin, M. (2013) Secretory defect and cytotoxicity: the potential disease mechanisms for the retinitis pigmentosa (RP)-associated interphotoreceptor retinoid-binding protein (IRBP). *J. Biol. Chem.* **288,** 11395–11406 CrossRef Medline
83. Sato, K., Li, S., Gordon, W. C., He, J., Liou, G. I., Hill, J. M., Travis, G. H., Bazan, N. G., and Jin, M. (2013) Receptor interacting protein kinase-mediated necrosis contributes to cone and rod photoreceptor degeneration in the retina lacking interphotoreceptor retinoid-binding protein. *J. Neurosci.* **33,** 17458–17468 CrossRef Medline
84. Jin, M., Li, S., Nusinowitz, S., Lloyd, M., Hu, J., Radu, R. A., Bok, D., and Travis, G. H. (2009) The role of interphotoreceptor retinoid-binding protein on the translocation of visual retinoids and function of cone photoreceptors. *J. Neurosci.* **29,** 1486–1495 CrossRef Medline